THE ASTROPHYSICAL JOURNAL, 432:690–700, 1994 September 10

CHROMOSPHERIC HEATING AND METAL DEFICIENCY IN COOL GIANTS: THEORETICAL RESULTS VERSUS OBSERVATIONS

M. CUNTZ[1]
High Altitude Observatory and Advanced Study Program, National Center for Atmospheric Research,[2] P.O. Box 3000, Boulder, CO 80307-3000

AND

W. RAMMACHER AND P. ULMSCHNEIDER
Institut für Theoretische Astrophysik, Universität Heidelberg, Im Neuenheimer Feld 561, D-69120 Heidelberg, Germany
Received 1993 November 24; accepted 1994 March 17

ABSTRACT

We compute acoustic shock wave–heated chromosphere models for moderately cool giant stars which differ greatly in metallicity. Subsequently, we simulate the emerging Mg II *k* lines assuming partial redistribution. The initial acoustic energy fluxes and the wave periods are taken from acoustic wave generation calculations based on traditional convection zone models. We find that the Mg II and Ca II core emissions are close to the observed basal flux limits which are common for giants and dwarfs. In addition, we find that the Mg II core emission is independent of the metallicity, in agreement with observations. We argue that these results should be considered as further evidence that the basal flux limits are indeed due to acoustic shock heating. The acoustic heating mechanism seems to be dominant in all nonmagnetic nonpulsating late-type stars.

Subject headings: hydrodynamics — shock waves — stars: abundances — stars: chromospheres — stars: giants — waves

1. INTRODUCTION

For many years it has been thought that the chromospheres of cool stars are dominantly heated by magnetic-field–related mechanisms. This view was based on the observational results that for most stars the chromospheric emission flux is closely correlated with the stellar rotation rate, which in turn is tightly correlated with the magnetic flux at the stellar surface (see, e.g., the review by Linsky 1991, and references therein). Since the late 1980s, however, this picture has changed considerably (see reviews by Ulmschneider 1990, 1993).

Schrijver (1987a, b) and Rutten et al. (1991) presented a detailed statistical analysis of flux-flux and flux-color relations derived from selected emission lines for a large sample of late-type stars. They found, particularly from their Mg II and Ca II emission line studies, that the statistical correlations can best be understood when the stellar emission line fluxes are assumed to consist of two components: a "basal" flux, which is independent of stellar rotation, and a "magnetic" flux, which depends on rotation and age. The basal flux could unequivocally be identified as an intrinsic property of the stars and is not an artifact of the detection limits. Well-defined basal flux limits were also found for other lines like C II, Si II, C IV, and Si IV, which, except for dwarf stars, are likewise not affected by the *IUE* detection limits. Stars which only have the basal flux component are usually referred to as chromospheric basal flux stars. Schrijver argued that, since the chromospheric flux is independent of the magnetic field, it can best be attributed to pure acoustic heating. Today, this is still the most tempting picture. Nevertheless, it cannot be ruled out entirely that even the basal flux stars have some remaining magnetic fields and thus might be magnetically heated. This option however never gained support by detailed model calculations.

Middelkoop (1982), who analyzed the Ca H and K lines of a total of 335 evolved stars, mostly giants, has already provided strong evidence for chromospheric basal flux limits. In particular he showed (his Fig. 4) that toward greater $B-V$ color, except for supergiants, all stars lie on a basal flux limit. The precise location of the basal flux limits has been investigated by Schrijver (1987a, b) and Rutten et al. (1991). Additional results were provided by Judge & Stencel (1991) who empirically analyzed global thermodynamic properties of the outer atmospheres and winds of evolved late-type stars. They showed that in particular nonpulsating M-type (super-) giants can be considered as chromospheric basal flux stars, because the relatively weak chromospheric emission of these stars depends only on their effective temperatures. This study, as well as that of Mathioudakis & Doyle (1992) on M-dwarf stars, allowed an extrapolation of Schrijver's basal flux limits to lower effective temperatures. Judge & Stencel also showed that the concept of determining the basal chromospheric emission flux breaks down for stars with major pulsation modes, particularly Miras, as the Mg II and Ca II emission closely follows the stellar pulsation cycles. An observational study targeting the transition between both types of stars was given by Judge et al. (1993).

Another observational feature which suggests the separation into two distinct chromospheric heating components is the spread in chromospheric emission activity. Magnetic heating, due to the variation of the stellar rotation rates, generates a wide spread of chromospheric emission fluxes for the same type of stars (see, e.g., Rutten 1987). Acoustic heating, however, always gives roughly the same emission flux for stars of the same effective temperature and gravity, thus leading to no or only narrow spreads in chromospheric activity. As a consequence, a wide spread of the chromospheric emission activity is a clear indication that magnetic heating occurs. Already Middelkoop (1982) showed that for his hotter stars there is a con-

[1] Also Joint Institute for Laboratory Astrophysics, University of Colorado and National Institute of Standards and Technology.

[2] The National Center for Atmospheric Research is sponsored by the National Science Foundation.

siderable spread in chromospheric activity, while for the cool stars, as mentioned above, only the narrow spread in basal flux emission is seen. The decrease of this spread in chromospheric activity with decreasing $B-V$, toward F stars, is well documented (Rutten 1987, Fig. 1; Walter & Schrijver 1987, Fig. 1). This can be explained by the two-component heating picture in a straightforward manner: The acoustic heating component, as derived from acoustic wave generation calculations of Bohn (1981, 1984), increases strongly toward decreasing $B-V$ and increasingly overwhelms the magnetic heating component. Here a strong nonspread emission component is added to a widespread emission component and thereby reduces the resulting spread. In other words, the acoustic heating component is expected to dominate in many inactive cool stars, including F stars. That acoustic wave heating is consistent with the basal flux emission of M-dwarf stars has been found by Mathioudakis & Doyle (1992). In addition, Mullan & Cheng (1993, 1994) recently showed that acoustic shock wave heating can possibly explain both the Mg II and the H Lyα fluxes from the chromospheres of the least active M-dwarf stars. Note however that some of these results are based not on time-dependent wave calculations, but on the implementation of a time-independent energy dissipation law.

Another very important feature of the "chromospheric basal flux limits," largely overlooked by the scientific community, is the potential impact of different metal abundances ("the metallicity problem"). Schrijver (1987a, b), Rutten et al. (1991), as well as Judge & Stencel (1991) found that the basal flux limits are relatively sharp and unaffected by different metallicities. These limits are also found to be largely unaffected by differences in stellar gravity (i.e., they are essentially the same for giants and dwarfs for a given effective temperature). Despite the strong gravity dependence of the acoustic energy generation, this can be explained with the acoustic shock heating picture as shown by Ulmschneider (1989) using acoustic wave calculations, although his calculations would need a recomputation of the Mg II and Ca II line profiles using partial redistribution (PRD).

The metallicity problem, however, remains unexplained: Despite the fact that for some stars the metal abundances are reduced by a large factor, the Mg II and Ca II emissions remain the same. A drastic example was given by Dupree, Hartmann, & Smith (1990). The authors studied *IUE* observations for a total of 10 metal-deficient giant stars. All stars were Population II stars, with metal abundances lower by factors of $\sim$10–100 relative to the Sun. Nevertheless, the Mg II emissions were observed to be commensurate with the values found for disk giant (Population I) stars of similar color. Their Figure 4 shows that the emission-line fluxes are perfectly consistent with the Mg II basal flux limit considering the $\pm$30% error bars valid for these observations. The authors did not give an explanation for these results, but speculated that these stars might have additional atmospheric activity, due to pulsational modes and the resulting shock dissipation, which may enhance the otherwise reduced Mg II emission caused by the lack of Mg atoms. The fact that chromospheric emission is independent of the metal abundances is also consistent with the scaling laws of Ayres (1979), which were found to be valid for various semi-empirical chromosphere models based on *IUE* data.

Can this metallicity problem be understood on the basis of acoustic heating as well? It is the purpose of the present work to show that this is indeed the case. We want to demonstrate that the curious behavior of the chromospheric emission with varying metal abundance can be readily reproduced by models based on acoustic shock wave dissipation. This complements other studies, which show that acoustic heating can explain the chromospheric Mg II and Ca II basal flux limits of F, G, K, and M main-sequence stars (Buchholz & Ulmschneider 1994).

Our paper is structured as follows: In § 2, we discuss the hydrodynamic methods used, the computation of the spectral lines, the generation of the starting atmospheres in radiative equilibrium, and the acoustic energy generation. Section 3 gives our results and discussion. Conclusions are presented in § 4.

2. METHODS

2.1. *Hydrodynamic Computation*

The computation of acoustic waves has been discussed in previous papers of this series (Ulmschneider et al. 1977; Ulmschneider, Muchmore, & Kalkofen 1987; Schmitz, Ulmschneider, & Kalkofen 1985; Rammacher & Ulmschneider 1992) and therefore does not need to be described again in detail. The basic features of these computations include the following:

1. We adopt solutions of the one-dimensional hydrodynamics equations, which consist of the continuity equation, the momentum equation, and the energy equation. The solutions are obtained with the method of characteristics.
2. At the bottom of the atmosphere, we introduce sinusoidal waves generated by a piston. The waves are followed to the point of shock formation and beyond.
3. The shocks are treated as discontinuities and are allowed to grow to arbitrary strengths. Since we utilize the method of characteristics, there is no need to use numerical viscosity for the treatment of the shocks. The shocks are also permitted to overtake one another.
4. At the top of the atmosphere we use a transmitting boundary condition. Details about the implementation of the transmitting boundary condition into the method of characteristics used have been described by Ulmschneider (1986).
5. Radiative energy losses (and gains) are described by solving the radiation transfer equations in the H^- continuum as well as the Mg II k and H Lyα lines (as representative chromospheric emitters, assuming complete redistribution [CRD]). The radiative transfer equations are solved together with the statistical equilibrium equations for the non-LTE populations.
6. H^- (bound-free and free-free) was treated in non-LTE exactly as in Vernazza, Avrett, & Loeser (1981) except with an electron density table computed with Kurucz's ATLAS program using LTE. Different electron density tables have been computed for the different metal abundances used.
7. The Mg II k line cooling rate has been computed using a new operator-splitting method (Buchholz et al. 1994), which is more accurate and faster than the modified core-saturation method previously used by Rammacher & Ulmschneider (1992).
8. We have not considered molecules, as we are primarily interested in investigating a differential effect. We also did not consider molecules in the computation of the electron density tables.

Particular note is made that we have not treated the ionization of hydrogen consistently together with the equations of hydrodynamics. Specifically, we have not included the hydrogen ionization energy in the hydrodynamic energy equation.

Time-dependent ionization and recombination effects of hydrogen are also important (see, e.g., Kneer 1980; Carlsson & Stein 1992; among others), but have not been included either. Interestingly, both approximations are expected to change the thermal structure of the atmospheres in opposite directions: ignoring the ionization energy of hydrogen in the energy equation produces an atmosphere which is definitely too hot; however, including this term but omitting the advective term as well as the time-derivative term in the statistical hydrogen rate equations produces an atmosphere which is too cool, particularly in regions behind shocks. Nevertheless, it is our plan to include both effects in our hydrodynamics code, which is currently under development (Cuntz & Höflich 1994).

2.2. *Computation of the Line Profiles*

For our calculations of the non-LTE line source functions we used the line data of Kalkofen, Ulmschneider, & Schmitz (1984) and assumed two-level atoms. The background continua were computed using the ATLAS code of Kurucz. We note that emission-line fluxes and profiles can only be computed properly when effects due to PRD are considered (see, e.g., Judge 1990). As a representative chromospheric emitter we have calculated the Mg II k line. For this we utilized a new operator-splitting method developed by Ulmschneider (1994). The redistribution was computed using the R II function without additional CRD contributions, following Gouttebroze (1986). As the amount of numerical labor in the PRD computations is more than an order of magnitude larger, it was not possible to use PRD in our time-dependent wave calculations. Only after the acoustic wave calculations were completed, did we compute PRD line profiles for selected phases of the wave.

As already discussed in a previous paper (Ulmschneider et al. 1987), the task of solving the energy equation in an acoustic wave calculation requires the computation of the entire chromospheric cooling function, which consists of many lines and continua. Because of the limited computer power available, it is not feasible to simultaneously treat many lines and continua with our time-dependent method. We therefore rely on the following approach: together with the H^- losses we only treat the Mg II k and H Lyα line cooling, assuming CRD. These computations were performed with a new operator-splitting method given by Buchholz et al. (1994), which is fast and thus well suited for time-dependent applications. Using CRD leads to about a factor of 10 more line cooling than using PRD (Hünerth & Ulmschneider 1994) and thus very crudely incorporates the bulk of the chromospheric line emitters. This procedure (without Lyα) has been tested (Ulmschneider et al. 1987) for the Sun by comparison with the total cooling rate of the chromosphere model C of Vernazza et al. (1981). The additional Lyα losses contribute only at great heights, where the Mg line cooling becomes weak. However, Lyα cooling is nevertheless useful in our present work because it dampens the large pulsational oscillations, which would otherwise develop into strong shocks. This approach is likely a source of systematic errors, particularly in the outer most regions of our models, but appears to be reasonable, since it does not affect the regions of Mg II line cooling very much.

For our wave computations with different element abundances, we change the electron density table, which was used for the H^- computation and in the routines for the Mg II k calculation as well as for the computation of the background opacities. We consider a total of three cases. First, we use solar abundances. Second and third, we decrease the abundances of all elements except H and He by one and two orders of magnitude, respectively. These cases are henceforth called $A_\odot$, $A_\odot/10$, and $A_\odot/100$, respectively. As solar Mg abundance we take $A_{\rm Mg} = 3.9 \times 10^{-5}$ (Kalkofen et al. 1984).

2.3. *Computation of the Initial Atmospheres*

For our acoustic wave calculations, we need starting atmospheres in radiative equilibrium because otherwise the atmospheres, after starting the time-dependent treatment, would show motions even in the absence of waves. To generate starting atmospheres, we use the same equations as in the hydrodynamic code, use the same height grid, and employ the same radiation treatment. The procedure of generating an initial atmosphere model consists of two steps. In the first step, a gray initial atmosphere model for a given radiative flux $F_{\rm rad} = \sigma T_{\rm eff}^4$ and gravity g is computed. Here the optical depth at the bottom of the atmosphere is specified, as is the height grid and the gas pressure at the top of the atmosphere. The second step is to bring this atmosphere to nongray radiative equilibrium.

In our earlier work we let the gray atmosphere model develop into a radiative equilibrium model by a time-dependent treatment. By taking the velocity to be zero at the bottom and using the time-dependent code, we generated an atmosphere model, where the motions quieted down to values of a few tens of centimeters per second. This procedure worked well for atmospheres which were not very extended, but ran into difficulties for more extended atmospheres. The reason in our case is that large deviations of the gray atmosphere from radiative equilibrium initiate motions which generate strong shocks. These transient shocks delivered a large amount of heat to the upper regions of the atmosphere, so that the cooling processes considered remain insufficient to radiate it away in a reasonable computational time span.

For this reason we modify the Unsöld correction procedure to bring the initial gray atmosphere to radiative equilibrium in a time-independent manner. On basis of the gray model, using the nongray non-LTE radiation treatment described in the subsections above, the radiative transfer equation is solved for H^- and the Mg II k line, providing values for the mean intensities J_ν and fluxes F_ν at every height z in an atmosphere which extends from $z = 0$ to $z = z_{\rm top}$. Subsequently temperature corrections are computed:

$$\Delta T(z) = \frac{1}{4\sigma T^3}\left[\frac{3}{4}\frac{\chi_5}{\mu}\int_0^z \Delta F(z')dz' + \frac{1}{2}\Delta F(z_{\rm top}) - \frac{T\rho\mu}{4\chi_5} D(z)\right]. \tag{2.1}$$

Here $F(z)$ is the frequency-integrated flux, χ_5 the opacity at 5000 Å, $\Delta F(z) = F(z) - F_{\rm rad}$, and D the radiation damping function (Ulmschneider et al. 1977, 1987)

$$D(z) = \frac{4\pi}{\rho T}\int_0^\infty \chi_\nu(J_\nu - S_\nu)d\nu = -\frac{1}{\rho T}\frac{\partial F}{\partial z}. \tag{2.2}$$

From the new temperatures, new values J_ν and F_ν are computed, and the procedure is repeated until the maximum change of ΔT becomes smaller than a given limit (e.g., 0.5 K). We find that then D is reduced to values less than 1% of the starting values and the wave motions to a few centimeters per second.

The crucial requirement in this process is the appropriate choice of the radiative boundary conditions. At the upper boundary, this is trivial: the specific intensities $I_\nu^-(z_{\rm top})$ are set

to zero for all frequencies for the ingoing radiation. At the lower boundary, however, the incident intensity $I_\nu^+(0)$ for the outgoing radiation has to be determined self-consistently. This is no problem for the Mg II k line, where the optical thickness at the photospheric level is so large that $I_\nu^+(0)$ can be chosen highly arbitrarily, e.g., such that $J_\nu(0) = S_\nu(0)$. For H^-, however, this approximation is bad since $\tau \approx 1$.

We use a set of two equations to determine $I_\nu^+(0)$ self-consistently. For our two-beam approximation we have for the total radiative flux at the bottom

$$F(0) = \sum_\nu 2\pi\mu[I_\nu^+(0) - I_\nu^-(0)]w_\nu , \qquad (2.3)$$

where w_ν is the set of frequency-angle integration weights. Usually $F(0)$ is not equal to $F_{\rm rad}$. To enforce a total flux of $F_{\rm rad}$ at the bottom, we multiply all intensities in equation (2.3) [henceforth called I_ν^+(old) and I_ν^-(old)] by a factor $f = F_{\rm rad}/F(0)$. From this we get

$$I_\nu^+(\text{new}) - I_\nu^-(\text{new}) = f[I_\nu^+(\text{old}) - I_\nu^-(\text{old})] . \qquad (2.4)$$

As the second equation we use equation (2.2) noting that in radiative equilibrium the damping function D is zero. Neglecting the frequency weighting by χ_ν yields, in the two-beam approximation,

$$I_\nu^+(\text{new}) + I_\nu^-(\text{new}) = 2S_\nu(\text{new}) . \qquad (2.5)$$

Here S_ν(new) is the source function of H^-, computed using the new temperature distribution, but keeping the departure coefficient b_{H^-} of the last iteration. Equations (2.4) and (2.5) can be solved for the unknowns

$$I_\nu^+(\text{new}) = \frac{f}{2}[I_\nu^+(\text{old}) - I_\nu^-(\text{old})] + S_\nu(\text{new}) . \qquad (2.6)$$

With these new incident intensities, the whole correction cycle is repeated until convergence is reached. Figure 1 shows the intensities I_ν^+(new) as a function of wavelength with the iteration number as parameter. The iteration is started using a Planck intensity distribution for $I_\nu^+(0)$ as initial guess. Fast convergence is easily achieved if the optical depth at the bottom is not too small.

Figure 2 shows the temperature distribution $T_{\rm re}$ and the extent of the radiative-equilibrium starting atmosphere models of our three cases. It is seen that the top of the models is strongly influenced by the metal abundances employed. With decreasing metal abundance, the Cayrel effect in H^- produces a successively more pronounced non-LTE temperature increase with atmospheric height. In atmospheres with greater metal abundance, this spatial temperature increase is usually counteracted by line cooling. Therefore, in the case with solar abundance, the Cayrel effect is reduced to a small side effect. Also the region below the temperature minimum is affected by the metallicity. Here the electrons necessary for the formation of H^-, which usually come from metals which are easy to ionize, do now originate from the very temperature-sensitive hydrogen ionization equilibrium. Note that with higher temperatures in the upper atmosphere, the density scale height becomes larger as does, therefore, the extent of the atmosphere.

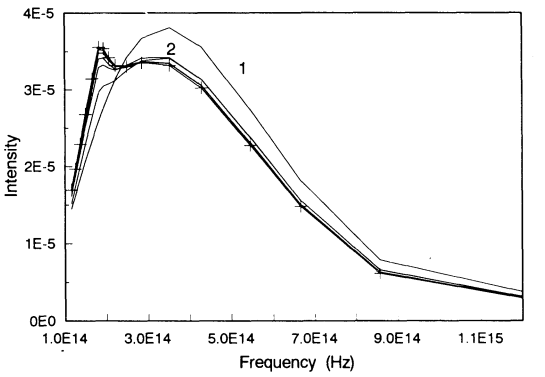

FIG. 1.—Successive iterations of the incident intensity I^+ at the bottom of the atmosphere as a function of wavelength for the giant star with solar abundance, during a temperature-correction procedure for a radiative-equilibrium starting atmosphere. The first six iterations are shown as is the twenty-first, indicated by + signs.

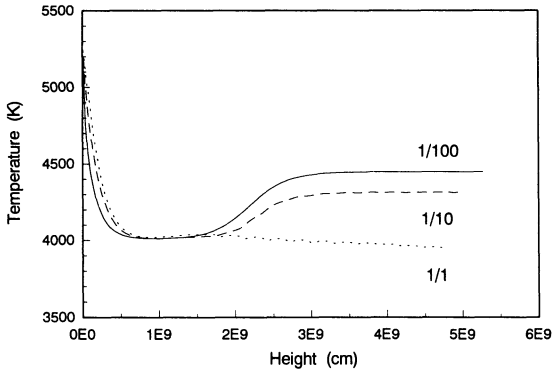

FIG. 2.—Temperature distribution of the radiative-equilibrium starting atmospheres for our three giant stars with $A_\odot$, $A_\odot/10$, and $A_\odot/100$.

2.4. *Acoustic Energy Generation*

The energy flux and spectrum of acoustic waves generated in the convection zone of stars other than the Sun cannot be observed but must be computed theoretically. The most advanced theoretical method to compute acoustic wave generation from the turbulent motions in stellar convection zones is the theory of Stein (1967, 1968), which is an extension of Lighthill's (1952, 1954) theory of aerodynamic sound generation by turbulence, developed for terrestrial industrial applications. Lighthill's theory, which contains as essential core the quadrupole sound generation term, has been very successfully tested and confirmed in experiments of jet noise generation. Stein's theory and its background has recently been rediscussed by Musielak et al. (1994) in the case of the Sun. They found that the older version of Stein's theory (Bohn 1981, 1984) gives basically realistic results, except that, due to unrealistic assumptions about the spatial and temporal parts of the turbulent energy spectrum, it overestimates the magnitude of the acoustic wave generation considerably. As the extension of Musielak et al.'s work to stars other than the Sun is presently unavailable, we have to resort to using Bohn's results. In particular, Bohn's basic result, that quadrupole sound generation is dominant in late-type giants as it is in the Sun, will remain unchanged.

The basic problem with applying Stein's theory to a stellar convection zone is that we need to know the turbulent velocity as a function of depth. However, for computing stellar convection in most types of stars, only the mixing-length concept is currently available. This approach needs the specification of the mixing-length parameter α, which is the ratio of the mixing length to the pressure scale height. As found by Bohn (1984), the acoustic flux depends on the mixing-length parameter as

$\alpha^{2.8}$, which for choices between $\alpha = 1$ and $\alpha = 2$ amounts to an uncertainty of a factor of 7. From Bohn's figures, we derive the mechanical energy fluxes $F_M = 2.2 \times 10^8$ and 7.6×10^8 ergs cm^{-2} s^{-1} for $\alpha = 1.0$ and 1.5, respectively, by taking the data of our giant star, which are log $T_{\rm eff} = 3.7$ and log $g = 3$. For comparison we derive $F_M = 1.8 \times 10^8$ and 6.8×10^8 ergs cm^{-2} s^{-1} for the Sun using log $T_{\rm eff} = 3.76$ and log $g = 4.45$ and $\alpha = 1.0$ and 1.5, respectively. Note that in this case, the α dependence for the giant as well as the Sun is considerably larger than Bohn's quoted value of 2.8, although not as large as the recent value of 3.8 (Musielak et al. 1994).

Because from time-dependent convection zone calculations, large convective velocities are found relatively close to the solar surface (Steffen 1992, private communication), we think a value of $\alpha = 2$ is most realistic for the Sun. For $\alpha = 2$, Musielak et al. (1994) find $F_M = 1.7 \times 10^8$ and 1.2×10^8 ergs cm^{-2} s^{-1} for the Sun by adopting two versions of the turbulent energy spectrum, representing an extended and a broadened Kolmogorov spectrum, respectively, with a modified Gaussian frequency factor in both cases. If we consider these values as the best values currently available for the Sun, we can try to correct Bohn's values for the giant. These values are much too large for $\alpha = 2$, due to the usage of the unrealistic exponential energy spectrum with an exponential frequency factor, which had been chosen to maximize acoustic fluxes and was not based on physical arguments (see Musielak et al. 1994). By scaling Bohn's giant/Sun ratios with our solar results we find acoustic fluxes of $F_M = 1.5 \times 10^8$ and 2.1×10^8 ergs cm^{-2} s^{-1}, respectively, for $\alpha = 2$. Because we want to perform our wave calculations with a fixed acoustic flux value, we choose $F_M = 2.0 \times 10^8$ ergs cm^{-2} s^{-1} as typical for our giant in the case of $A_\odot$.

The acoustic flux generation is influenced by the chemical composition. From Bohn's (1984) Figure 8 we derive a value of $F_M = 1.8 \times 10^8$ ergs cm^{-2} s^{-1} for a giant if a mixture $A_\odot/10$ is used. This is a reduction of 20% relative to the case $A_\odot$. However, recent convection zone calculations of Theurer (1993), who used improved gray opacities extending to relatively low atmospheric temperatures using the tables of Alexander, Johnson, & Rypma (1983) and Alexander, Augason, & Johnson (1989), show that the acoustic energy fluxes are only marginally metallicity sensitive. While using the Lighthill formula and $\alpha = 2$, he found that the acoustic fluxes change very little, from $F_M = 2.15 \times 10^8$ to 2.08×10^8 ergs cm^{-2} s^{-1} for the mixtures $A_\odot$ and $A_\odot/100$, respectively. Due to this result we decided to assume the same acoustic flux for all three cases $A_\odot$, $A_\odot/10$, and $A_\odot/100$. Note incidentally that the pure Lighthill formula appears to give acoustic fluxes surprisingly similar to the much more advanced Stein theory.

It remains to discuss the acoustic spectrum. Musielak et al. (1994) showed that for the Sun the acoustic spectrum extends from the acoustic cutoff frequency $\omega_A = 3.0 \times 10^{-3}$ Hz to roughly a factor of 10 higher, reaching a smooth, pronounced maximum at about 0.015 Hz or a period of $P = 60$ s for $\alpha = 2$. Although acoustic waves of considerable energy with periods down to 40 s are observed on the Sun (see Ulmschneider 1990 for a discussion of these temporal observations), it is puzzling that recent time-dependent convection zone calculations do not reproduce such short-period waves (Steffen 1994). Steffen essentially finds a spectrum which peaks in the 3 minute region and rapidly decreases to greater frequency. As pointed out by Steffen (1993, private communication) this result could be due to the—compared with the Kolmogorov law—much steeper turbulent energy spectrum found in his two-dimensional computations. The Kolmogorov law is observed to be valid on solar spatial scales (Zahn 1987; Muller 1989) and was employed in the calculations of Musielak et al. (1994).

As both the temporal and spatial solar observations point to the existence of short-period wave modes, we are encouraged to adopt the solar acoustic wave spectra of Musielak et al. (1994). Bohn (1981) computed a large number of acoustic wave spectra of stars in the H-R diagram, shown also by Ulmschneider (1991). These spectra are very similar in shape to the recent solar spectra, with a similarly smooth and pronounced peak at $\omega = 5\omega_A$. Because we want to use monochromatic acoustic waves for our time-dependent wave calculations, we therefore adopt wave periods of $P = P_A/5 = 1120$ s for our model atmospheres, where $P_A = 4\pi c/\gamma g = 2\pi/\omega_A$ is the acoustic cutoff period. Note that this is different from Ulmschneider (1989), who used $P = P_A/10$.

3. RESULTS AND DISCUSSION

3.1. *Three Acoustically Heated Giant Models*

We now discuss our hydrodynamic models in detail. We take the three initial radiative equilibrium models (see Fig. 2) and introduce acoustic waves of period $P = 1120$ s and energy flux $F_M = 2.0 \times 10^8$ ergs cm^{-2} s^{-1} by piston motion. The dissipation of energy creates acoustically heated chromospheres, of which Figures 3–5 show snapshots at roughly the same phase. Note that the three giant-star chromosphere models have metal abundances of $A_\odot$, $A_\odot/10$, and $A_\odot/100$, respectively. It is seen that the temperature and velocity amplitudes as well as the time-averaged temperatures $T_{\rm av}$ in the three models are very similar up to roughly a height of 3.0×10^9 cm. The zero-height point is defined as the level where the optical depth $\tau_{5000} = 1.3$. Because time averaging was performed over a time span of only one wave period to the phases shown, the averaged temperature $T_{\rm av}$ (similar to other averaged quantities not given in our figures) is very noisy and should be taken only as an estimate. At great heights $T_{\rm av}$ is also affected by pulsation modes, which occur on longer timescales.

Figures 3–5 show that the temperature minimum occurs in all three cases roughly at the height 1.0×10^9 cm. That the

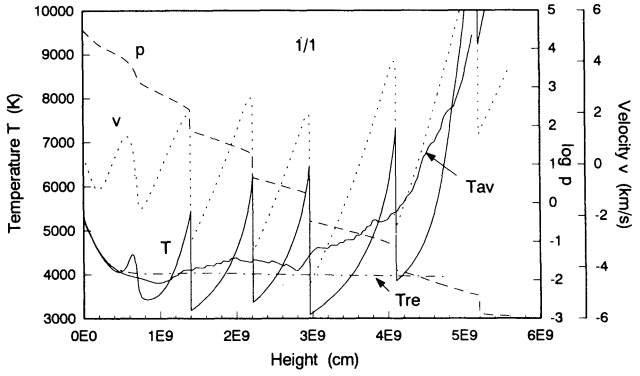

FIG. 3.—Acoustic wave–heated atmosphere model of a giant star with $T_{\rm eff} = 5012$ K and gravity $g = 1.0 \times 10^3$ cm s^{-2} at time $t = 2.193 \times 10^4$ s. The star has solar metal abundance; the wave has a period of $P = 1120$ s and an initial energy flux of $F_M = 2.0 \times 10^8$ ergs cm^{-2} s^{-1}. Shown versus height are the temperature T, the time-averaged temperature $T_{\rm av}$, the radiative equilibrium temperature $T_{\rm re}$ of the initial atmosphere, the velocity v, and the gas pressure p (in dyn cm^{-2}).

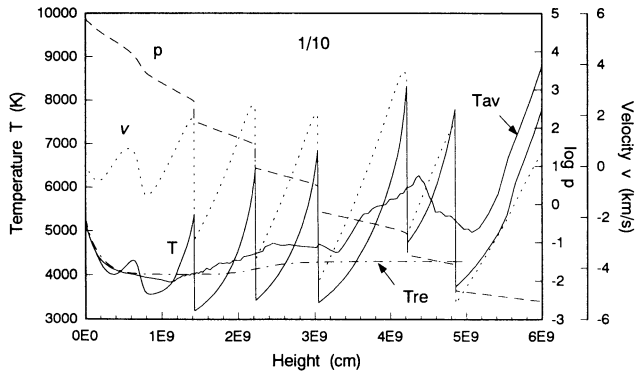

FIG. 4.—Same as Fig. 3, except for a star with 1/10 solar metal abundance at time $t = 2.186 \times 10^4$ s.

temperature minimum is lower than it is in the radiative equilibrium atmosphere is a well-known feature of all acoustic wave models (Ulmschneider et al. 1977) and is due to the nonlinearity of the Planck function. Up to the height 3.0×10^9 cm the time-averaged temperature T_{av} closely follows the radiative equilibrium temperature T_{re} with a deviation of 300 K at most. This constitutes an essentially isothermal region, which extends over five orders of magnitude in gas pressure. That the acoustic heating, other than in the Sun, does not lead to a strong chromospheric temperature rise is a consequence of the much more efficient radiation damping in a giant-star atmosphere (see Ulmschneider 1988).

The temperature and velocity jumps at the shocks are similar in all three cases. This is a consequence of the limiting shock strength behavior, which for a given wave period P and gravity g produces shocks of similar strength, independent of the gas pressure and of other quantities, including the metal abundances (see, e.g., Cuntz & Ulmschneider 1988; Ulmschneider 1991). Once the shocks are fully developed, the shock strengths essentially do not change with atmospheric height. Note however that the situation is different when the assumption of monochromatic waves is dropped in favor of a detailed treatment of an acoustic frequency spectrum (e.g., Cuntz 1987; Fleck & Schmitz 1993). In this case, persistent shock-shock interaction occurs, producing different shock strengths at a given atmospheric height. The study of acoustic frequency spectra, however, is beyond the scope of our present paper.

At heights above 3.0×10^9 cm the effect of pulsation, excited by the initiation of the wave calculation and maintained by shock overtaking, is present. These oscillations occur despite radiation damping by Lyα as discussed by Rammacher & Ulmschneider (1992) and are most obvious in the behavior of the velocity. Figure 3 shows a strong outflow, where as an inflow is seen in Figure 4. These pulsations are also partly responsible for the perturbations of the averaged temperatures T_{av} at these heights. Another cause for these perturbations is the decrease of the efficiency of the Mg II line cooling with height, while the Lyα cooling is restricted to the greatest heights only. Particularly in the case $A_\odot/100$ (see Fig. 5) this effect leads to a peak in the average temperature near 3.6×10^9 cm.

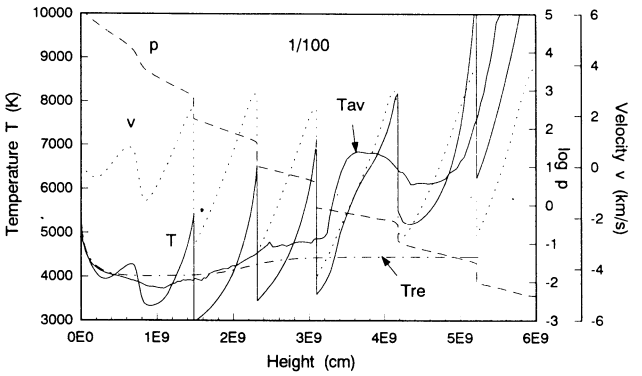

FIG. 5.—Same as Fig. 3, except for a star with 1/100 solar metal abundance at time $t = 2.076 \times 10^4$ s.

At the heights above 5.0×10^9 cm, the temperature rises steeply in all three models. The reason for this temperature rise is well understood and is attributable to unbalanced heating, when a major chromospheric cooling mechanism, here the Lyα line cooling, vanishes because of hydrogen ionization (Ulmschneider et al. 1987; Rammacher & Ulmschneider 1992). Continued imbalance between heating and cooling leads to the formation of a transition layer where the persistent time-dependent heating generates an even steeper temperature rise by switching off the remaining hydrogen line cooling more quickly by ionizing the hydrogen atom. Note however that adequately handling this process requires a multilevel treatment of hydrogen ionization including the solution of the time-dependent rate equations, which is also not within the scope of this paper.

Figures 3–5 also show that for a given height the mean gas pressures are different in the three cases considered. It is a factor of 2.4 higher in Figure 4 than in Figure 3 and another factor of 1.9 higher in Figure 5 than in Figure 4. This pressure increase is a consequence of our definition of the zero-height level in our atmospheres. A lower metal abundance reduces the opacity, and thus one has to go to higher column mass densities of the atmosphere, i.e., to higher gas pressure, in order to reach an optical depth of 1.3.

3.2. Mg II *k* Line Profiles

Using the methods described above we have computed the Mg II k line profiles both in the CRD and PRD approximation. The CRD profiles have been computed only for tutorial purposes. The emergent intensities for the atmospheres of Figures 3–5 are shown in Figures 6–8, respectively. As the lines emerging from our bumpy atmospheres vary with the phase of the acoustic wave, line profiles were computed also for other phases. Figures 6–8, in addition, show line profiles for wave phases which occur a time span $\Delta t = P/2 = 560$ s earlier. Because of the narrowness of the PRD line profiles, we bunch our frequency points there and display the profiles only over the wavelength range ± 2 Å.

The comparison of Figures 6–8 shows that the width of the emission peaks strongly decreases toward lower metal abundance both for the CRD and the PRD profiles. This is due to the fact that the line opacity, being proportional to the Mg II number density, decreases in proportion with the Mg abundances. For a given wavelength in the line wing one essentially sees the source function at the height level where the optical depth is near unity at this wavelength. As with lower metal abundance, the optical depth in the line wing decreases, one sees, to higher column mass densities of the atmosphere for a given wavelength. Therefore, the wavelengths where one observes the temperature minimum, that is the k_1 intensity

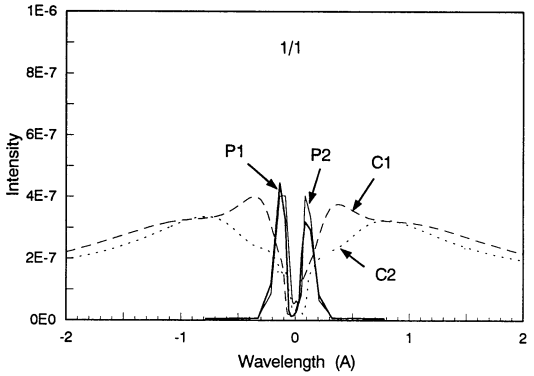

FIG. 6.—Mg II k line intensities (ergs cm^{-2} s^{-1} sr^{-1} Hz^{-1}) as function of wavelength difference (Å) from line center for the giant star with solar metal abundance. "P1" and "C1" label PRD and CRD line profiles for the wave phase shown in Fig. 3. "P2" and "C2" label PRD and CRD profiles for a wave phase by a time span of $\Delta t = P/2 = 560$ s earlier than those in Fig. 3.

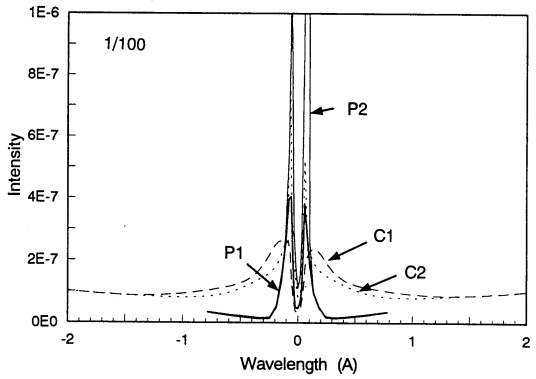

FIG. 8.—Same as Fig. 6, except for the star with 1/100 solar metal abundance shown in Fig. 5.

minima in the lines, move close to the line center with decreasing metallicity.

Why is the dependence of the width of the emission core (between the k_1 minima) on the metallicity so much larger for the CRD profiles than for the PRD profiles? The CRD lines have extended wings because the line core photons can migrate across the width of the line due to the CRD assumption, and they get emitted far in the wings. Therefore, even at great depth there is a significant emission of photons, which closely follows the source function and contributes to the large overestimation of the line cooling already discussed above. Due to the moderate wavelength dependence of the Lorentz profile, a lowering of the metal abundance rapidly decreases the wavelength difference k_1 from line center (i.e., 6.6, 3.1, and 1.4 Å for CRD in the models $A_\odot$, $A_\odot/10$, and $A_\odot/100$, respectively), where the minimum of the source function is seen, and thus quickly narrows the width of the emission core.

In PRD, on the other hand, the photons are not allowed to migrate over much more than the width of the Doppler core. This width includes both the thermal Doppler width and the "wave turbulence" width due to the Doppler shifts of the core by the velocity amplitude of the wave. This combined Doppler width, which is in the range of about ± 4 thermal Doppler widths, neither changes much as function of height in the three stars (see Figs. 3–5), nor changes much from one star to the other. Therefore, the PRD emission does not show a large wavelength dependence, as reflected in our results.

3.3. Mg II *and* Ca II *Emission Fluxes*

Integrating the emission cores of the Mg II k lines over wavelengths between the k_1 minima yields the total emergent emission intensities I_k^+. These emission intensities have been converted to the emission fluxes F_k using $F_k = 2\pi I_k^+/\sqrt{3}$ for our two-beam approximation with angle cosine $\mu = 1/\sqrt{3}$. Since we are interested in the total Mg II flux we also have to consider the contribution of the Mg II h lines. In the optically thin case, we would have to multiply the flux of Mg II k by a factor of 1.5, because $F_k:F_h = 2:1$. As we do not have an optically thin case, this procedure would lead to unrealistic results. A way of solving this problem is to consider detailed observational results. Stencel et al. (1980) have measured Mg II h and k flux ratios for a sample of 54 cool stars. On average, they found $F_k:F_h = 1.3:1$. Therefore, our Mg II k fluxes should best be multiplied by a factor of 1.8 to get reasonable Mg II h plus k emission estimates when detailed multilevel calculations are unavailable. The total Mg II emission fluxes $F_{Mg} = F_h + F_k$ thus obtained are given in Table 1. A similar procedure was used to estimate the total Ca II H plus K fluxes. The results are given in Table 2. In this case, we used a factor of 2 to convert the Ca II K line flux into the total Ca II emission flux. Note however that this procedure is also very crude. Note that

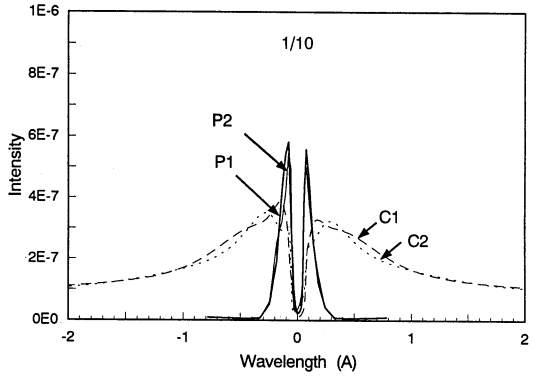

FIG. 7.—Same as Fig. 6, except for the star with 1/10 solar metal abundance shown in Fig. 4.

TABLE 1

Mg II COOLING RATE (ergs cm^{-3} s^{-1})

Star	$t^{(i)}$	$t^{(i)} - P/2$	Average
$A_\odot$	5.43	5.45	5.44
$A_\odot/10$	5.52	5.50	5.51
$A_\odot/100$	5.26	5.69	5.53

TABLE 2

Ca II COOLING RATE (ergs cm^{-3} s^{-1})

Star	$t^{(i)}$	$t^{(i)} - P/2$	Average
$A_\odot$	6.13	6.11	6.12
$A_\odot/10$	6.03	6.03	6.03
$A_\odot/100$	5.84	5.84	5.84

observational studies similar to that for Mg II are missing or contain results which cannot be used. The reason is that observed Ca II fluxes are usually strongly contaminated by photospheric contributions which differ with the spectral type and luminosity class of the star. In addition, the calibration of the continuum flux at the position of the Ca II H and K lines is often relatively uncertain, particularly when detailed model atmospheres do not exist.

We note that the PRD Mg II fluxes do not show any dependence on the metal abundances. The reason for this is that the PRD emission is tied to the Doppler core. Lowering the metal abundance by factors of 10 or 100 acts like moving the emitting region downward to parts of the atmosphere where the density is greater by a factor of 10 to 100. Due to the small scale height of the atmosphere, this is not a large distance. Taking a mean temperature of $T = 4500$ K we obtain a density scale height of $H = \Re T/\mu g = 2.9 \times 10^8$ cm. Decreasing the metal abundance by a factor of 10 or 100 thus corresponds to lowering the scale heights by factors of 2.3 or 4.6, which is a distance Δh of 6.7×10^8 or 1.3×10^9 cm, respectively. To show this in more detail we have plotted the heights where the optical depth τ is unity versus wavelength. Figure 9 shows these τ-unity surfaces for the $A_\odot$ and $A_\odot/100$ cases. It is seen that τ-unity at line center reaches a maximum height of 5×10^9 cm in both cases, here the Gauss profile dominates the opacity. Away from the line center the height of the τ-unity surface rapidly decreases when the Lorentz profile of the damping wings dominates the opacity. In addition, a case $A_\odot/100$ is shown in which we artificially raised the abundances back to the solar value in the otherwise unchanged atmosphere model of Figure 5. The height difference of the τ-unity surfaces of the two $A_\odot/100$ cases is seen to be indeed as estimated above.

Being closely tied to the Doppler core, the bulk of the PRD emission, which in the $A_\odot$ case arises from a region around 3.5×10^9 cm, is shifted downward in the $A_\odot/100$ case to a region around 2.0×10^9 cm as a consequence of the abundance decrease by a factor 100. Over these height ranges, however, as seen from Figures 3–5, the temperature and velocity structure of the atmospheres is not very much height dependent. Note that because the emission comes mainly from the hot postshock regions, the temperature and velocity amplitude of the wave is also important. The surprisingly small metallicity dependence of the Mg II PRD line emission can thus be explained by the similarity of the wave shape (the temperature and velocity amplitude) over a considerable span of the quasi-isothermal height regions in the acoustically heated giant chromospheres.

As already discussed above, the similarity of the wave amplitudes is due to the limiting shock strength behavior (see, e.g., Cuntz & Ulmschneider 1988; Ulmschneider 1991) which, also called shape similarity invariance, is a general property of acoustic shock waves (Brinkley & Kirkwood 1947). However, this constant-strength shock wave could in principle (as, e.g., in the case of the Sun) propagate over a strongly increasing ambient temperature distribution. For the similarity of the Mg II line emission in our cases with different metallicity it is important that the time average temperature does not show a large height dependence. It is precisely the quasi-isothermal mean atmosphere already discussed above which is essential for the missing metallicity dependence of the Mg II emission. This quasi-isothermal atmosphere region in giants is due to the more efficient radiative cooling (see Ulmschneider 1988), which forces the average temperature T_{av} to be close to the radiative equilibrium temperature T_{eq} in these stars.

We now compare our results with observations. In Figure 10 we plotted the averaged total Mg II emission fluxes of Table 1 into Figure 1*b* of Rutten et al. (1991). It is seen that our PRD fluxes satisfy reasonably well the observed common basal flux limit for giants and dwarfs. The fact that the Mg II emission in dwarf stars is also in agreement with the chromospheric basal flux limit has recently been shown by Buchholz & Ulmschneider (1994), who computed wave models for F, G, K, and M

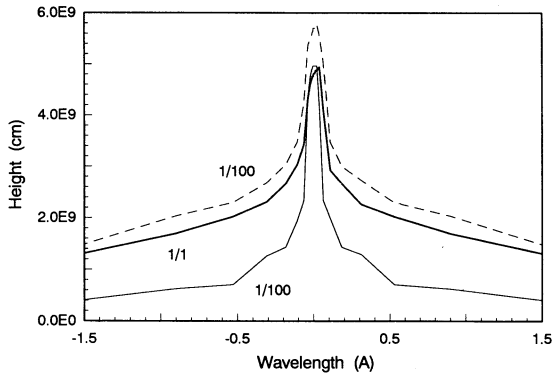

FIG. 9.—Atmospheric heights where the optical depth is unity for the models of Fig. 3 (1/1) and Fig. 5 (1/100) as function of wavelength for the Mg II *k* line. Also shown for the model of Fig. 5 is the case (*dashed*) in which the Mg metal abundance has been artificially raised back to the solar value.

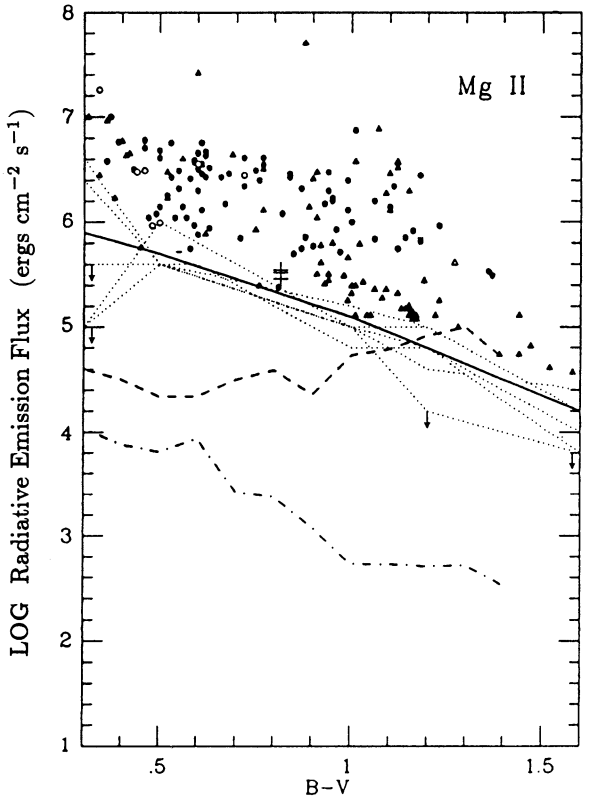

FIG. 10.—Theoretical emission fluxes of Mg II *h* and *k* lines based on acoustic wave models for giants with different metal abundances compared with empirical fluxes by Rutten et al. (1991). The theoretical emission fluxes are indicated by crosses.

main-sequence stars. As our results depend on a long chain of reasoning, the agreement with observation to within a factor of 2 should be considered satisfactory. Note that the CRD emission fluxes, which are 6.77, 6.39, and 5.94 (in logarithmic cgs units) for the wave models with $A_\odot$, $A_\odot/10$, and $A_\odot/100$, respectively, would show a strong metallicity dependence which is not observed and would also not fit the chromospheric basal flux values. This behavior demonstrates again that the CRD approximation is inappropriate for this type of study and should be avoided.

Figure 11 shows the averaged total Ca II emission fluxes of Table 2 plotted into Figure 1*a* of Rutten et al. In this case, the chromospheric basal flux line could also be reproduced to some extent. However, contrary to the Mg II results, a slight but significant metallicity dependence of the Ca II emission exists. We strongly feel that this behavior does not necessarily weaken our conclusions, since emission from Ca II is much more likely to be affected by multilevel radiative transfer effects than is the case for Mg II emission. In addition, the Ca II K line fluxes cannot be converted into Ca II H plus K fluxes in a straightforward manner.

Besides the omission of treating multilevel radiative transfer in Mg II and Ca II, we have to realize that our results are affected by various technical restrictions in the code and distinct uncertainties of input parameters. As discussed above, we started from a considerable uncertainty about the acoustic energy generation due to uncertainties in the stellar convection zone model and the theory of Stein. Fortunately, the impact of these uncertainties is reduced considerably by the limiting strength behavior of the acoustic waves and by the strong radiation damping in the giant-star atmosphere. These effects lead to extended quasi-isothermal regions which would also occur if the initial acoustic energy fluxes were considerably higher or lower. The principal radiative losses occur in the photosphere and lower chromosphere and are primarily caused by H^-. In typical cases, Mg II is formed at higher atmospheric layers and remains therefore unaffected by the initial acoustic energy flux adopted. Note however that a more detailed discussion should also consider the influence of the acoustic wave spectrum, which will be one of our future research projects.

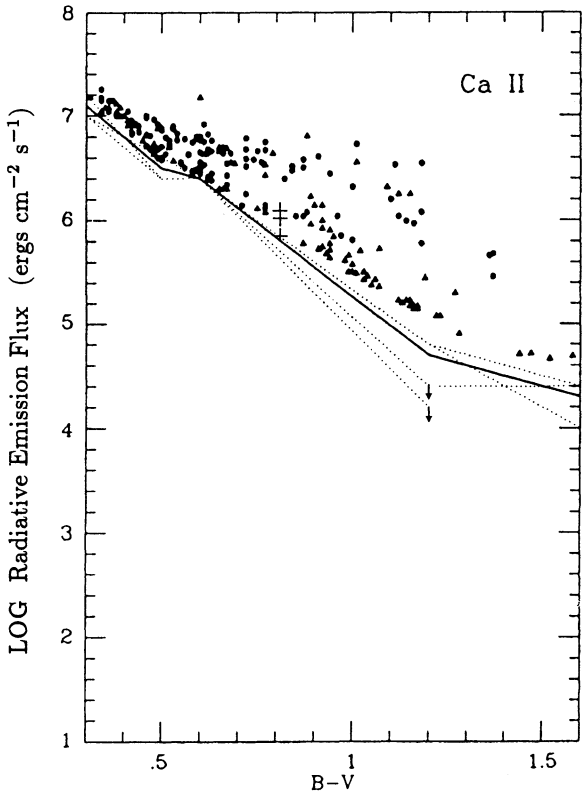

FIG. 11.—Same as Fig. 10, but for emission fluxes of Ca II H and K lines.

4. CONCLUSIONS

We computed radiation-hydrodynamic models for the chromospheres of moderately cool giant stars based on acoustic shock wave heating and subsequently simulated the Mg II *k* line emission assuming PRD. Line profiles based on CRD were also computed for tutorial purposes to demonstrate that CRD is an inappropriate approximation which should be avoided. For the stellar parameters, we took $T_{\rm eff} = 5012$ K and $g = 10^3$ cm s^{-2}. The acoustic wave generation calculations of Bohn (1981, 1984) were scaled using recent results of Musielak et al. (1994) for the Sun. We derived an initial acoustic wave flux of $F_{\rm M} = 2.0 \times 10^8$ ergs cm^{-2} s^{-1} and a wave period of $P = P_A/5 = 1120$ s representing the peak of the acoustic energy spectrum. For the metallicity abundances, we used $A_\odot$, $A_\odot/10$, and $A_\odot/100$, which gave us a grid of three giant-star chromosphere models. We found:

1. Chromospheric heating is a common feature in all three giant models. Over a distance of about 5 orders of magnitude in pressure (up to a height of about 3×10^9 cm measured above optical depth $\tau_{5000} = 1.3$), extended, quasi-isothermal atmospheres with mean temperatures of about 4500 K are found.

2. The time-averaged temperatures in these isothermal regions are close to the radiative equilibrium temperatures of the initial atmosphere, being 300 K higher at most. Above the height 3×10^9 cm, the chromospheric temperatures are affected by pulsational motions initiated by shock-overtaking similar to those found by Rammacher & Ulmschneider (1992) for the Sun. Above 5×10^9 cm, the temperatures rise steeply and eventually form transition layers.

3. The base of the chromosphere, which is close to the point of shock formation, is roughly at height 1×10^9 cm and is found to be almost identical in all models.

4. The atmospheric temperatures are slightly higher (< 300 K) in models with lower metallicity. This is mainly due to radiative heating by the Cayrel effect and is already present in the initial radiative equilibrium models.

5. In models with lower metallicity, the optical depth of the Mg II *k* line is reduced, and the line is formed at higher column mass densities, where due to the extended isothermal region similar temperatures, velocities, and Mg II particle densities, but higher total particle densities, are found.

6. Most significantly, our models explain two distinct observational facts. First, it was found that, although Population I and II stars differ in metallicity by up to a factor of 100, the Mg II emission in these stars is observed to be almost identical (Dupree et al. 1990). Second, there is a common basal flux limit for giants and dwarfs for Mg II and Ca II emission. This limit is relatively sharp and remains unaffected by element abundances. Up to now the underlying cause of these results

remained unexplained. We show that all these effects can readily be reproduced by our models. The emerging time-averaged PRD Mg II emission line fluxes are virtually identical for our wave models with $A_\odot$, $A_\odot/10$, and $A_\odot/100$. These results show that although the metal abundances are reduced by a factor of 100, the changes in the emerging Mg II emission line fluxes are insignificant.

7. Our PRD emission fluxes also lie close to the common basal flux limit for giant and dwarf stars for Mg II and Ca II emission. We found that the Mg II and Ca II PRD fluxes satisfy the observed basal flux within a factor of 2. Our result is more strong evidence that the chromospheres of basal flux stars are indeed heated acoustically and should be considered together with the strong support for this interpretation given by Ulmschneider (1989) and Buchholz & Ulmschneider (1994). The latter authors have shown that acoustic heating can probably explain the chromospheric Mg II and Ca II basal flux limits of F, G, K, and M main-sequence stars.

8. Contrary to the case for Mg II, a slight but significant metallicity dependence of the Ca II emission exists. Note however that we do not trust our Ca II results completely since Ca II emission is much more likely to be affected by multilevel radiative transfer effects than is the case for the Mg II emission. In addition, the Ca II K line fluxes cannot be converted into Ca II H plus K fluxes in a straightforward manner.

The reason that the Mg II emission in our models remains unaffected by metal abundances is threefold: First, the mean chromospheric temperature is slightly higher in models with lower metallicity, which helps to increase the Mg II emission flux. Second, and most important, in models with lower metallicity the optical depth in the Mg II *k* line (which was treated as a representative chromospheric emitter) is reduced, forcing the line to be formed at higher column mass densities, where larger total-particle densities are found. As a consequence, the reduced metal abundance is compensated. Third, because of the limiting shock strength behavior of the waves (see, e.g., Cuntz & Ulmschneider 1988) the wave shape (i.e., temperature and velocity amplitude) is the same in large portions of all three model atmospheres, allowing the Mg II *k* line to be formed under similar thermodynamic conditions.

Dupree et al. (1990) speculated that metal-pure giant stars might have additional atmospheric activity due to pulsational modes to offset the otherwise reduced Mg II emission. This speculation now seems unnecessary. Also note that this suspicion gained temporary support from other studies, including the observation of low-amplitude radial velocity variations in α Boo (K1.5 III), a metal-poor old disk population star (e.g., Cochran 1988). The fact that chromospheric emission is independent of the metal abundances is also consistent with the scaling laws of Ayres (1979), which are found to be valid for various semiempirical chromosphere models based on *IUE* data. Because our results depend on a long chain of reasoning where it is likely that uncertainties and technical restrictions in the codes accumulate, the agreement with observation both for Mg II and Ca II to within a factor of 2 appears satisfactory. Note that this discrepancy is much smaller than the uncertainty in the initial acoustic energy flux employed. Also note that changing the initial acoustic flux would not have a significant effect on the emerging Mg II emission flux, because of the limiting shock strength property of the waves and the strong radiation damping in the atmosphere, which in photospheric layers mainly occurs in H^-. Nevertheless, all these results will be reviewed using a more sophisticated radiation hydrodynamics code which is in preparation.

Despite our encouraging results, at least two issues related to the heating of chromospheric basal flux stars are still unresolved. First, it is observed that cool-star chromospheres are highly inhomogeneous, in part probably due to CO/SiO radiative instabilities, reducing the filling factor of the hot chromospheric component significantly (e.g., Wiedemann & Ayres 1990). Second, the magnitude of chromospheric turbulence is unexplained. Recent *HST*-GHRS data for α Tau (K5 III), which is also a well-known chromospheric basal flux star, revealed a high level of turbulence in the chromosphere (i.e., $\simeq 24$ km s^{-1}) (Carpenter et al. 1991), which is inconsistent with "traditional" acoustic heating models (Judge & Cuntz 1993). Nevertheless, we believe that our results are a key to attributing chromospheric basal flux limits to acoustic heating. Acoustic heating is probably dominant in all nonmagnetic nonpulsating late-type stars.

We would like to thank Mats Carlsson and P. G. Judge for valuable comments on an earlier version of the manuscript. M. C. acknowledges financial support through the Advanced Study Program at the National Center for Atmospheric Research and through NASA grant NAG W-2904 to the University of Colorado. He also acknowledges a travel grant through the SFB 328 Evolution of Galaxies provided by the Deutsche Forschungsgemeinschaft. W. R. and P. U. acknowledge support by the Deutsche Forschungsgemeinschaft through project Ul 57/16-1.

Note added in manuscript.—In a very recent paper, Dupree et al. (1994) presented observational results for chromospheric emission in two red giant stars (A31 and A59), which are members of the globular cluster NGC 6752. The results have been obtained with the Goddard High Resolution Spectrograph. Dupree et al. found that the Mg II emission in these stars is perfectly consistent with the chromospheric basal flux limit given by Rutten et al. (1991). Dupree et al. also reported asymmetries in the line profiles of the Mg II and Hα lines, which they interpret as a spectroscopic signature for propagating shocks. Both results can be viewed as further support for the basic conclusions of this paper.

REFERENCES

Alexander, D. R., Augason, G. C., & Johnson, H. R. 1989, ApJ, 345, 1014
Alexander, D. R., Johnson, H. R., & Rypma, R. L. 1983, ApJ, 272, 773
Ayres, T. R. 1979, ApJ, 228, 509
Bohn, H. U. 1981, Ph.D. thesis, Univ. Würzburg
———. 1984, A&A, 136, 338
Brinkley, S. R., & Kirkwood, J. G. 1947, Phys. Rev., 71, 606
Buchholz, B., Hauschildt, P., Rammacher, W., & Ulmschneider, P. 1994, A&A, 285, 987
Buchholz, B., & Ulmschneider, P. 1994, in Cool Stars, Stellar Systems, and the Sun, Proc. 8th Cambridge Workshop, in preparation
Carlsson, M., & Stein, R. F. 1992, ApJ, 397, L59
Carpenter, K. G., Robinson, R. D., Wahlgren, G. M., Ake, T. B., Ebbets, D. C., Linsky, J. L., Brown, A., & Walter, F. M. 1991, ApJ, 377, L45
Cochran, W. D. 1988, ApJ, 334, 349
Cuntz, M. 1987, A&A, 188, L5
Cuntz, M., & Höflich, P. 1994, in preparation
Cuntz, M., & Ulmschneider, P. 1988, A&A, 193, 119
Dupree, A. K., Hartmann, L., & Smith, G. H. 1990, ApJ, 353, 623
Dupree, A. K., Hartmann, L., Smith, G. H., Rodgers, A. W., Roberts, W. H., & Zucker, D. B. 1994, ApJ, 421, 542
Fleck, B., & Schmitz, F. 1993, A&A, 273, 671
Gouttebroze, P. 1986, A&A, 160, 195

Hünerth, G., & Ulmschneider, P. 1994, A&A, in press
Judge, P. G. 1990, ApJ, 348, 279
Judge, P. G., & Cuntz, M. 1993, ApJ, 409, 776
Judge, P. G., Luttermoser, D. G., Neff, D. H., Cuntz, M., & Stencel, R. E. 1993, AJ, 105, 1973
Judge, P. G., & Stencel, R. E. 1991, ApJ, 371, 357
Kalkofen, W., Ulmschneider, P., & Schmitz, F. 1984, ApJ, 287, 952
Kneer, F. 1980, A&A, 87, 229
Lighthill, M. J. 1952, Proc. Royal Soc. A, 211, 564
———. 1954, Proc. Royal Soc. A, 222, 1
Linsky, J. L. 1991, in IAU Colloq. 130, The Sun and Cool Stars: Activity, Magnetism, Dynamos, ed. I. Tuominen et al. (Lecture Notes in Physics 380) (Berlin: Springer), 452
Mathioudakis, M., & Doyle, J. G. 1992, A&A, 262, 523
Middelkoop, F. 1982, A&A, 113, 1
Mullan, D. J., & Cheng, Q. Q. 1993, ApJ, 412, 312
———. 1994, ApJ, 420, 392
Muller, R. 1989, in Solar and Stellar Granulation, ed. R. J. Rutten & G. Severino (Dordrecht: Kluwer), 101
Musielak, Z. E. 1991, in Mechanisms of Chromospheric and Coronal Heating, ed. P. Ulmschneider et al. (Berlin: Springer), 369
Musielak, Z. E., Rosner, R., Stein, R. F., & Ulmschneider, P. 1994, ApJ, 423, 474
Rammacher, W., & Ulmschneider, P. 1992, A&A, 253, 586
Rutten, R. G. M. 1987, A&A, 177, 131
Rutten, R. G. M., Schrijver, C. J., Lemmens, A. F. P., & Zwaan, C. 1991, A&A, 252, 203
Schmitz, F., Ulmschneider, P., & Kalkofen, W. 1985, A&A, 148, 217
Schrijver, C. J. 1987a, A&A, 172, 111
———. 1987b, in Cool Stars, Stellar Systems, and the Sun, Proc. 5th Cambridge Workshop, ed. J. L. Linsky & R. E. Stencel (Berlin: Springer), 135
Steffen, M. 1994, in Solar Magnetic Fields, ed. M. Schüssler & W. Schmidt (Cambridge: Cambridge Univ. Press), in press
Stein, R. F. 1967, Solar Phys., 2, 385
———. 1968, ApJ, 154, 297
Stencel, R. E., Mullan, D. J., Linsky, J. L., Basri, G. S., & Worden, S. P. 1980, ApJ, 44, 383
Theuer, J. 1993, Diploma thesis, Univ. Heidelberg
Ulmschneider, P. 1986, A&A, 168, 308
———. 1988, A&A, 197, 223
———. 1989, A&A, 222, 171
———. 1990, in Cool Stars, Stellar Systems, and the Sun, Proc. 6th Cambridge Workshop, ed. G. Wallerstein (ASP Conf. Ser., 9), 3
———. 1991, in Mechanisms of Chromospheric and Coronal Heating, ed. P. Ulmschneider et al. (Berlin: Springer), 328
———. 1993, in Advances in Stellar and Solar Coronal Physics, ed. J. L. Linsky & S. Serio (Dordrecht: Kluwer), 533
———. 1994, A&A, in press
Ulmschneider, P., Kalkofen, W., Nowak, T., & Bohn, H. U. 1977, A&A, 54, 61
Ulmschneider, P., Muchmore, D., & Kalkofen, W. 1987, A&A, 177, 292
Vernazza, J. E., Avrett, E. H., & Loeser, R. 1981, ApJS, 45, 635
Walter, F. M., & Schrijver, C. J. 1987, in Cool Stars, Stellar Systems, and the Sun, Proc. 5th Cambridge Workshop, ed. J. L. Linsky & R. E. Stencel (Berlin: Springer), 262
Wiedemann, G., & Ayres, T. R. 1990, in Cool Stars, Stellar Systems, and the Sun, Proc. 6th Cambridge Workshop, ed. G. Wallerstein (ASP Conf. Ser., 9), 158
Zahn, J.-P. 1987, in Lecture Notes in Physics 292, Solar and Stellar Physics, ed. E. H. Schröter & M. Schüssler (Berlin: Springer), 55